Optica Applicata, Vol. XXXI, No. 2, 2001

Selectivity properties of circular grating DFB/DBR lasers with phase shift

PAWEŁ SZCZEPAŃSKI

Institute of Microelectronics and Optoelectronics Warsaw University of Technology, ul. Koszykowa 75, 00–662 Warszawa, Poland. National Institute of Telecommunications, ul. Szachowa 1, 04–894 Warszawa, Poland.

SYLWIA TARASIUK

Institute of Microelectronics and Optoelectronics, Warsaw University of Technology, ul. Koszykowa 75, 00–662 Warszawa, Poland.

A threshold analysis is presented for circular grating distributed feedback (CG-DFB) and circular grating distributed Bragg reflector (CG-DBR) lasers with additional phase shift introduced in the grating region. It is found that proper value and position of the additional phase shift reduce threshold gain of the laser structure and also improve its mode selectivity.

1. Introduction

Surface-emitting circular grating distributed feedback (CG-DFB) and Bragg reflector (CG-DBR) lasers have received much attention in the past years [1]–[28]. These lasers are of interest primarily because they can deliver high-power, low-divergence circular beams. Moreover, in plane light propagation facilitates monolithic integration of the various grating and active elements to form functional and highly compact coherent light sources, as well as two-dimensional laser arrays.

The curved-line gratings as resonators and reflectors were initially suggested by TIEN [1]. Next, ZAHENG [2] applied circular gratings as two-dimensional resonators. SHINO *et al.* [3] and HORI *et al.* [4] designed and fabricated focusing grating mirror. Shimpe patented cylindrical diffraction grating couplers and distributed feedback resonators [5]. Circular gratings could be used in leak-wave antenna [6], which when combined with active materials, would be a new type of surface-emitting lasers.

Circular grating could also serve as a multipart directional coupler [7], [8], which might be especially useful in multichannel operation. In addition to circular gratings, elliptic Bragg gratings have been also proposed by SUDBO [9] for application in integrated optics.

The first optically pumped surface-emitting CG-DFB laser was demonstrated in 1991 [10]. In this case the second-order grating for both optical feedback and

outcoupling was used. Similar cavity configuration was applied in optically pumped [11], [12] and electrically pumped [13]–[17] CG-DFB and CG-DBR lasers. More recently, an electrically pumped CG-DBR laser with an integrated outcoupler has been developed [18]–[21]. This laser consists of a central first order-grating DBR resonator surrounded by independent chirp outcoupling grating which focuses emitting light (or shapes required pattern of the output light beam).

Simultaneously, a theoretical analysis of the properties of circular grating devices has been carried out [22]–[29]. In particular, a detailed, vector-wave formulation of self-consistent coupled-wave theory for circular waves, applicable to both passive and active circular grating devices formed on dielectric waveguides, has been provided [25]. It has been shown that for gratings having cylindrical symmetry, only circular waves of the same order are coupled. Moreover, for zero-order cylindrical waves, pure TE-TE (or TM-TM) wave coupling occurs and for higher order waves, there is coupling between TE and TM modes. The threshold analysis [27] has shown that CG-DFB lasers normally have a higher threshold gain than CG-DBR lasers. Moreover, by a proper choice of the inner grating radius it is possible to select either even or odd waves.

More recently, an analysis of the above-threshold operation of CG-DFB laser has been reported [30]. Non-linear scalar coupled-mode equations taking into account gain saturation effect, but including only radial field distribution of the laser mode, have been solved numerically with a fourth order Runge–Kutta algorithm. The non-linear model of CG-BFB laser has been extended to take into account the coupling between partial waves, characteristic for the second order grating, and the effect of the power mode nonorthogonality [31].

Recently, an approximate method for analysing the non-linear operation of circular DBR laser has been developed [32]. This method is based upon vector-wave self-consistent coupled mode equations and includes a three-dimensional spatial field dependence of the laser modes. With the help of the energy theorem an the threshold field approximation an approximate formula relating small signal gain to the output power and laser parameters has been derived. Using this formula it is possible to investigate an influence of the real system parameters (*e.g.*, distributed losses, coupling strength of the grating, geometry of the resonator, *etc.*) on maximal power efficiency of the laser structure.

Much effort has also been focused on the mode discrimination [22], [29] in CG DFB/DBR laser structures. In particular, fundamental mode operation could be obtained [22] when the periodicity and the position of the grating are chosen in such a way that all of the reflections from each refractive index step are superimposed in phase, so as to be self-consistent with the resonant behaviour of the fundamental wave. Another method of the mode selectivity has been proposed in [29]. It has been shown that a small perturbation introduced into the complex constant of the active region causes the suppression of the unwanted lateral modes of odd symmetry. Very recently, effects of radiation loss in second order circular grating DFB lasers have been studied [35], [36]. It has been shown that for sufficiently strong coupling radiative losses

improve mode selectivity [35]. Moreover, it was found that device and pump-beam parameters can have a significant effect on the threshold gains of the laser, as well as on the azimuthal mode discrimination and total lasing linewidth it exhibits [36].

In this paper, we investigate the effect of an additional phase shift introduced into the grating region on threshold gain and mode spectrum in DFB/DBR laser having circular grating. In general, it is a well established fact that in linear DFB laser structures the $\lambda/4$ grating shift provides a single mode operation at Bragg frequency [33]. However, in the case of circular grating DFB and DBR lasers the situation is more complex. We show that the additional phase shift can improve mode selectivity and decrease the threshold gain of the fundamental DFB (DBR) mode, but its optimal value and the position in the grating region strongly depend on the other laser parameters. Especially, the optimal value of the phase shift introduced is sensitive to the grating phase measuring the grating position with respect to the central point of the laser structure.

In the next section, coupled mode equations for CG-DFB/DBR laser structures with additional phase shift introduced are derived. In Section 3, threshold conditions for these lasers are formulated. The threshold characteristics for distributed feedback as well as Bragg reflector lasers revealing the influence of the additional phase shift on mode spectrum are discussed in Section 4. In the last section conclusions are drawn.

2. Coupled mode-equations for TE-circular waves

In circular grating devices, the propagation waves are inward and outward propagating cylindrical waves described by Hankel functions. According to the detailed vector-wave formulation of a self-consistent coupled-wave theory for cylindrical waves [25] the coupled-mode equations can be written in the following form:

$$p\frac{\mathrm{d}a_{\mu nq}^{(p)\sigma}(r)}{\mathrm{d}r} = -j\omega \frac{1}{\int_0^{2\pi}\int_{-\infty}^{\infty} r\mathrm{d}\theta\mathrm{d}z[\vec{E}_{\mu nt}^{(p)\sigma} \times \vec{H}_{\mu nt}^{(p)\sigma *} + \vec{E}_{\mu nt}^{(p)\sigma *} \times \vec{H}_{\mu nt}^{(p)\sigma}]\hat{r}} \times \int_0^{2\pi}\int_{-\infty}^{\infty} r\mathrm{d}\theta\mathrm{d}z\left\{\varepsilon_0\Delta\varepsilon\sum_{q,\tau,m} a_{vm}^{(p)\tau}(r)\left[\vec{E}_{vmt}^{(p)\sigma} + \frac{\varepsilon}{\varepsilon+\Delta\varepsilon}\vec{E}_{vmr}^{(p)\tau}\right]\right\}\vec{E}_{\mu m}^{(s)\sigma *} \qquad (1)$$

where ω is the optical frequency of light, ε_0 – the permittivity of vacuum, ε – the relative permittivity of an ideal planar waveguide, and $\Delta\varepsilon$ – the perturbation introduced by gain in the active region and by the circular grating in the Bragg reflector region. The E are the electric field components of the cylindrical wave in the ideal planar waveguide and $a_{\mu nq}^{(p)\sigma}(r)$ are slow varying mode amplitudes resulting from perturbation of the ideal waveguide. The subscript r denotes the r-th component of the field and the transverse θ- and z- components are denoted by t. In Equation (1) the subscript p (or s) represents

the outward cylindrical waves when $p = +$ (or $s = +$) and in-ward propagating waves when $p = -$ (or $s = -$). The polarization TE or TM of the waveguide modes is denoted by subscripts σ or τ, respecively. The subscripts ν and μ are the modal numbers of planar waveguide modes associated with the order of the cylindrical waves denoted by n or m (integral numbers), and q denotes an order of the DFB/DBR modes ("longitudinal" modes). The factor p on the left-hand side of relation (1) corresponds either to "+" for out-ward propagating cylindrical waves or to "–" for in-ward propagating waves. The asterisk in (1) represents the complex conjugate. According to [25] the field distributions of TE cylindrical modes of unperturbed planar waveguide are

$$E_{\mu nz}^{(p)\mathrm{TE}} = 0, \quad H = A_{\mu n}^{(p)\mathrm{TE}} R_n^{(p)}(\beta_\mu^{\mathrm{TE}} r) Z_\mu^{\mathrm{TE}}(z) e^{jn\theta}, \tag{2a}$$

$$E_{\mu nr}^{(p)\mathrm{TE}} = A_{\mu n}^{(p)\mathrm{TE}} \frac{n\omega\mu_0}{(\beta_\mu^{\mathrm{TE}})^2} \frac{1}{r} R_n^{(p)}(\beta_\mu^{\mathrm{TE}} r) Z_\mu^{\mathrm{TE}}(z) e^{jn\theta} = A_{\mu n}^{(p)\mathrm{TE}} \frac{n\omega\mu_0}{(\beta_\mu^{\mathrm{TE}})^2} \tilde{E}_{\mu nr}^{(p)\mathrm{TE}}, \tag{2b}$$

$$E_{\mu n\theta}^{(p)\mathrm{TE}} = A_{\mu n}^{(p)\mathrm{TE}} \frac{j\omega\mu_0}{(\beta_\mu^{\mathrm{TE}})^2} \frac{\mathrm{d}R_n^{(p)}(\beta_\mu^{\mathrm{TE}} r)}{\mathrm{d}r} Z_\mu^{\mathrm{TE}}(z) e^{jn\theta} = A_{\mu n}^{(p)\mathrm{TE}} \frac{j\omega\mu_0}{(\beta_\mu^{\mathrm{TE}})^2} \tilde{E}_{\mu n\theta}^{(p)\mathrm{TE}}, \tag{2c}$$

$$H_{\mu nr}^{(p)\mathrm{TE}} = A_{\mu n}^{(p)\mathrm{TE}} \frac{1}{(\beta_\mu^{\mathrm{TE}})^2} \frac{\mathrm{d}R_n^{(p)}(\beta_\mu^{\mathrm{TE}} r)}{\mathrm{d}r} \frac{\mathrm{d}Z_\mu^{\mathrm{TE}}(z)}{\mathrm{d}z} e^{jn\theta}, \tag{2d}$$

$$H_{\mu n\theta}^{(p)\mathrm{TE}} = A_{\mu n}^{(p)\mathrm{TE}} \frac{jn}{(\beta_\mu^{\mathrm{TE}})^2} \frac{1}{r} R_n^{(p)}(\beta_\mu^{\mathrm{TE}} r) \frac{\mathrm{d}Z_\mu^{\mathrm{TE}}(z)}{\mathrm{d}z} e^{jn\theta} \tag{2e}$$

where μ_0 is the permeability, $A_{\mu n}^{(p)\mathrm{TE}}$ is the field amplitude, $Z_{\mu n}^{\mathrm{TE}}(z)$ are the slab modes having propagation constant $\beta_{\mu n}^{\mathrm{TE}}$ (solutions for slab waveguides and dispersion relations for calculating $\beta_{\mu n}^{\mathrm{TE}}$ can be found in standard text books, see, for example, [33]), radial distributions for outward-propagating modes and inward -propagating modes are described by

$$R_n^{(+)}(\beta_\mu^{\mathrm{TE}} r) = H_n^{(2)}(\beta_\mu^{\mathrm{TE}} r) = J_n(\beta_\mu^{\mathrm{TE}} r) - jN_n(\beta_\mu^{\mathrm{TE}} r)$$

and

$$R_n^{(-)}(\beta_\mu^{\mathrm{TE}} r) = H_n^{(1)}(\beta_\mu^{\mathrm{TE}} r) = J_n(\beta_\mu^{\mathrm{TE}} r) + jN_n(\beta_\mu^{\mathrm{TE}} r),$$

respectively, where $H_n^{(1)}$ and $H_n^{(2)}$ are the Hankel functions of the first and second kind, respectively, J_n is the n-th order Bessel function of the first kind and N_n is the n-th order Neumann function.

We assume, similarly as in [25], [32], the small perturbation with $\Delta\varepsilon/(\varepsilon + \Delta\varepsilon) \ll 1$ and neglect interpolarization coupling, which is a consequence of the long radius approximation especially valid for DBR structure [32]. Moreover, we confine our analysis to the structures having grating of cylindrical symmetry, *i.e.*, $\Delta\varepsilon(r, \theta, z) = \Delta\varepsilon(r, z)$, in which only coupling between the cylindrical waves of the

same order occurs. Under these assumptions, with normalised field distribution (2) in such a way that

$$\int_0^{2\pi}\int_{-\infty}^{\infty} r\,\mathrm{d}\theta\,\mathrm{d}z[\vec{E}_{\mu nt}^{(p)\sigma}\times\vec{H}_{\mu nt}^{(p)\sigma *}+\vec{E}_{\mu nt}^{(p)\sigma *}\times\vec{H}_{\mu nt}^{(p)\sigma}]\hat{r}=1,$$

which results in $\left|A_{\mu n}^{\mathrm{TE}}\right|^2=\dfrac{(\beta_\mu^{\mathrm{TE}})^2}{8\omega\mu_0\int_{-\infty}^{\infty}\left|Z_\mu^{\mathrm{TE}}\right|^2\mathrm{d}z}$, the coupled mode Equations (1) can be rewritten for TE modes in the following form:

$$\frac{\mathrm{d}a_{\mu n}^{(+)\mathrm{TE}}}{\mathrm{d}r}=-j\sum_\nu K_{\mu\nu}^{\mathrm{TETE}}(r)\left[e^{j(\beta_\mu^{\mathrm{TE}}-\beta_\nu^{\mathrm{TE}})r}a_{\nu n}^{(+)\mathrm{TE}}+j(-1)^n e^{j(\beta_\mu^{\mathrm{TE}}+\beta_\nu^{\mathrm{TE}})r}a_{\nu n}^{(-)\mathrm{TE}}\right],$$

$$\frac{\mathrm{d}a_{\mu n}^{(-)\mathrm{TE}}}{\mathrm{d}r}=j\sum_\nu K_{\mu\nu}^{\mathrm{TETE}}(r)\left[-j(-1)^n e^{-j(\beta_\mu^{\mathrm{TE}}+\beta_\nu^{\mathrm{TE}})r}a_{\nu n}^{(+)\mathrm{TE}}+e^{-j(\beta_\mu^{\mathrm{TE}}-\beta_\nu^{\mathrm{TE}})r}a_{\nu n}^{(-)\mathrm{TE}}\right] \tag{3}$$

where the coupling coefficient is given by

$$K_{\mu\nu}^{\mathrm{TETE}}(r)=\frac{k_0^2}{2\sqrt{\beta_\mu^{\mathrm{TE}}\beta_\nu^{\mathrm{TE}}}}\frac{\int_{-\infty}^{\infty}\Delta\varepsilon(r,z)Z_\nu^{\mathrm{TE}}\mathrm{d}z}{\sqrt{\int_{-\infty}^{\infty}\left|Z_\mu^{\mathrm{TE}}\right|\mathrm{d}z\int_{-\infty}^{\infty}\left|Z_\nu^{\mathrm{TE}}\right|\mathrm{d}z}}. \tag{4}$$

Next, assuming that circular grating is fabricated on a single-mode planar waveguide, the coupled-wave equations for TE-cylindrical waves (Eq. 4) are:

$$\frac{\mathrm{d}a_n^{(+)}}{\mathrm{d}r}=-jK(r)[a_n^{(+)}(r)+j(-1)^n e^{j2\beta r}a_n^{(-)}(r)],$$

$$\frac{\mathrm{d}a_n^{(-)}}{\mathrm{d}r}=jK(r)[-j(-1)^n e^{-j2\beta r}a_n^{(+)}(r)+a_n^{(-)}(r)] \tag{5}$$

where the coupling coefficient $K_{\mu\nu}^{\mathrm{TETE}}$ given by Eqs. (3) with $\beta_\mu^{\mathrm{TE}}=\beta_\nu^{\mathrm{TE}}=\beta$.

In the next section, we use relations (5) as a starting point for threshold analysis of CG-DFB/DBR lasers with the phase shift. In Section 4, threshold conditions for these laser structures are formulated.

3. Eigenvalue equation for circular grating lasers with phase shift

We consider a laser structure such as shown schematically in Fig. 1. The device is composed of a uniform central region of radius R_1 and surrounding grating region $R_1 < r < R_3$, where R_3 is the outer radius of the circular grating. The phase shift of the grating in introduced at $r = R_2$. In the case of CG-DFB laser, the active medium extends over the whole grating region. In the case of CG-DBR laser, the active material is limited within the central region of radius R_1 and the grating region is passive.

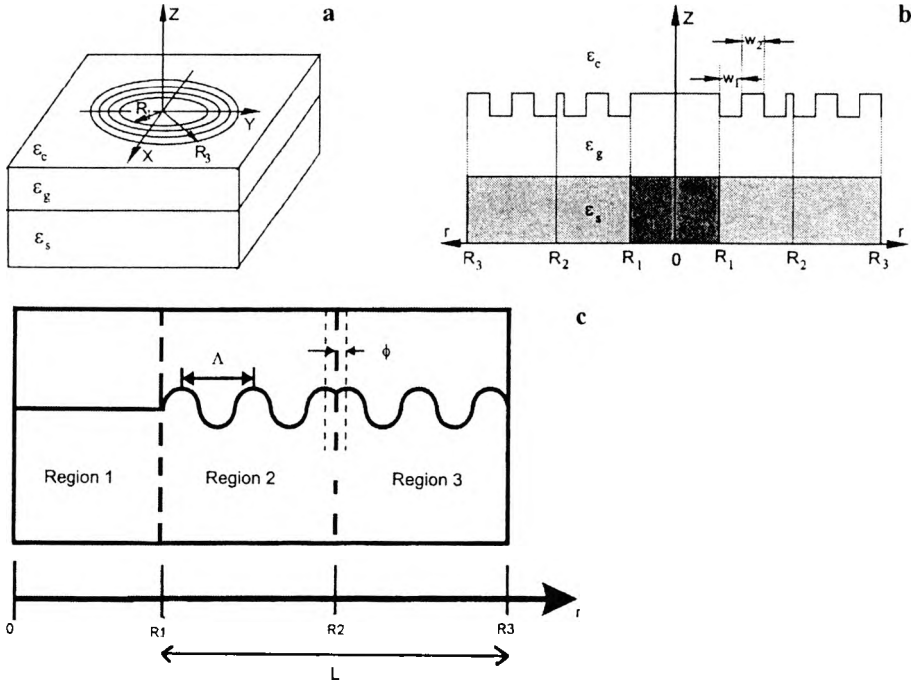

Fig. 1. Diagram of circular grating (CG) laser with phase shift introduced: schematic view (**a**), and cross-sections (**b**, **c**).

The cross-section of the CG-laser is depicted in Fig. 2, where without loss of generality, the circular grating is assumed to have a rectangular profile. The line spacing of the grating is denoted by W_1, the line width by W_2, and the grating period by Λ ($\Lambda = W_1 + W_2$).

The eigenvalue equations for CG lasers can be derived by solving Eqs. (5) with specific boundary conditions. First, we should find the coupling coefficient $K(r)$. Since a CG laser is composed of a central region (active medium-uniform waveguide) and a grating region, the equivalent unperturbed waveguide for these two regions should be different. Thus, in our approach we choose the unperturbed waveguides for central region and the grating region as two different waveguides. When the phase shift is introduced into the grating region it can be easily shown that the coupling coefficient for CG-DBR structure can be written in the following form:

$$K(r) = j\alpha_1 \quad \text{for} \quad 0 < r < R_1, \tag{6a}$$

$$K(r) = j\alpha_2 - \sum_{m=-\infty}^{+\infty} K_m e^{-j\Omega_m} e^{j\left(\frac{2\pi}{\Lambda}\right)mr} e^{j\phi} \quad \text{for} \quad R_1 < r < R_2, \tag{6b}$$

$$K(r) = j\alpha_2 - \sum_{m=-\infty}^{+\infty} K_m e^{-j\Omega_m} e^{j\left(\frac{2\pi}{\Lambda}\right)mr} e^{-j\phi} \quad \text{for} \quad R_2 < r < R_3, \tag{6c}$$

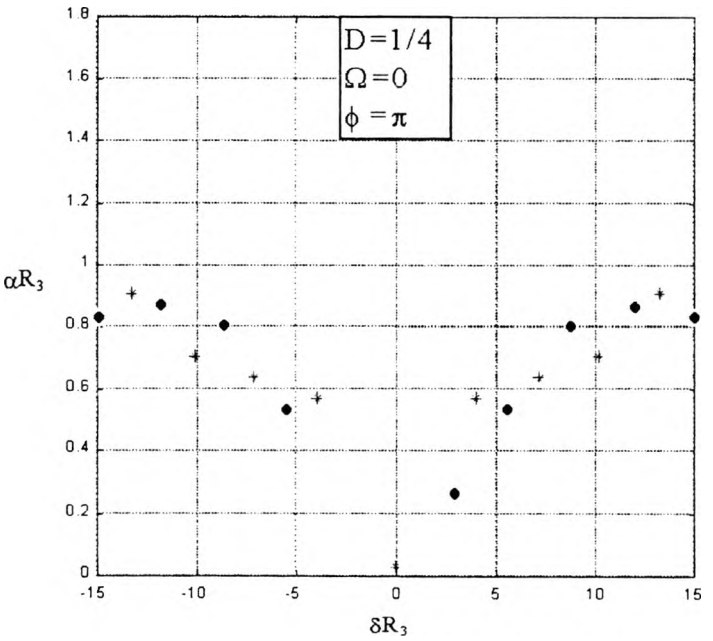

Fig. 2. Mode spectrum of CG-DFB laser with $K_m R_2 = 1.0$, $D = 1/4$, and (Ω, ϕ) equal $(0, \pi)$.

The gain in the central region $(0 < r < R_1)$ and the loss in the grating region $(R_1 < r < R_3)$ are denoted by α_1 and α_2, respectively. In the case of CG DFB structure $\alpha = \alpha_1 = \alpha_2$ denotes gain, and $R_1 = r$. The K_m is the m-th order coupling coefficient of the grating, Ω_m is a phase constant (describing the position of the grating with respect to the centre of the structure), and ϕ denotes the phase shift introduced into the grating region at $r = R_2$.

3.1. Solution for $0 < r < R_1$

By substituting Eq. (6a) into Eq. (5), the coupled mode equations for $0 < r < R_1$ become:

$$\frac{da_n^{(+)}}{dr} = \alpha_1[a_n^{(+)}(r) + j(-1)^n e^{j2\beta r} a_n^{(-)}(r)],$$

$$\frac{da_n^{(-)}}{dr} = -\alpha_1[-j(-1)^n e^{-j2\beta r} a_n^{(+)}(r) + a_n^{(-)}(r)] \tag{7}$$

where β is the propagation constant of the unperturbed waveguide for the central region and α are the amplitudes of the counter-running cylindrical waves of the "longitudinal" laser modes. Neglecting the fast oscillating terms in Eqs. (7) and solving the resulting equations, we get

$$a_n^{(+)}(r) = a_n^{(+)}(0) e^{\alpha_1 r},$$

$$a_n^{(-)}(r) = a_n^{(-)}(0)e^{-\alpha_1 r},$$

which can be expressed in the matrix form in the following way:

$$\begin{bmatrix} a_n^{(+)}(r) \\ a_n^{(-)}(r) \end{bmatrix} = \begin{bmatrix} e^{\alpha_1 r} & 0 \\ 0 & e^{-\alpha_1 r} \end{bmatrix} \begin{bmatrix} a_n^{(+)}(0) \\ a_n^{(-)}(0) \end{bmatrix}, \quad 0 < r < R_1. \tag{8}$$

3.2. Solution for $R_1 < r < R_2$

For the first grating region, $R_1 < r < R_2$, substituting Eq. (6b) into Eqs. (5), we have

$$\frac{da_n^{(+)}}{dr} = -j\left[j\alpha_2 - \sum_{m=-\infty}^{+\infty} K_m e^{-j\Omega_m} e^{j\left(\frac{2\pi}{\Lambda}\right)mr} e^{j\phi}\right][a_n^{(+)}(r) + j(-1)^n e^{j2\tilde{\beta}r} a_n^{(-)}(r)],$$

$$\frac{da_n^{(-)}}{dr} = j\left[j\alpha_2 - \sum_{m=-\infty}^{+\infty} K_m e^{-j\Omega_m} e^{j\left(\frac{2\pi}{\Lambda}\right)mr} e^{j\phi}\right][-j(-1)^n e^{-j2\tilde{\beta}r} a_n^{(+)}(r) + a_n^{(-)}(r)] \tag{9}$$

where $\tilde{\beta}$ is the propagation constant of the unperturbed waveguide for the grating region. Let δ denotes the deviation from the Bragg frequency, $\delta = \tilde{\beta} - m\pi/\Lambda$. If $|\delta \ll 1|$, then only the resonant terms are important. By neglecting the fast oscillating terms in Eqs. (9), the coupled mode equations can be written as:

$$\frac{da_n^{(+)}}{dr} = \alpha_2 a_n^{(+)}(r) - (-1)^n K_m e^{j2\delta r} e^{j(\Omega_m + \phi)} a_n^{(-)}(r),$$

$$\frac{da_n^{(-)}}{dr} = -\alpha_2 a_n^{(-)}(r) - (-1)^n K_m e^{-j2\delta r} e^{-j(\Omega_m - \phi)} a_n^{(+)}(r). \tag{10}$$

The solution of Eqs. (10) can be obtained in the following matrix form:

$$\begin{bmatrix} a_n^{(+)}(r) \\ a_n^{(-)}(r) \end{bmatrix} = \begin{bmatrix} T'_{11}(r) & T'_{12}(r) \\ T'_{21}(r) & T'_{22}(r) \end{bmatrix} \begin{bmatrix} a_n^{(+)}(R_1) \\ a_n^{(-)}(R_1) \end{bmatrix}, \quad R_1 < r < R_2, \tag{11}$$

where the matrix elements are defined by:

$$T'_{11}(r) = e^{j\delta(r-R_1)}\left\{\cosh[\gamma_1(r-R_1)] + \frac{\alpha_2 - j\delta}{\gamma_1}\sinh[\gamma_1(r-R_1)]\right\}, \tag{12a}$$

$$T'_{12}(r) = \frac{\alpha_m}{\gamma_1} e^{j(\Omega_m + \phi)} e^{j\delta(r+R_1)} \sinh[\gamma_1(r-R_1)], \tag{12b}$$

$$T'_{21}(r) = \frac{\alpha_m}{\gamma_1} e^{-j(\Omega_m - \phi)} e^{-j\delta(r-R_1)} \sinh[\gamma_1(r-R_1)], \tag{12c}$$

$$T'_{22}(r) = e^{-j\delta(r-R_1)}\left\{\cosh[\gamma_1(r-R_1)] - \frac{\alpha_2 - j\delta}{\gamma_1}\sinh[\gamma_1(r-R_1)]\right\}, \tag{12d}$$

and the complex propagation constant is given by

$$\gamma_1 = \sqrt{\alpha_m^2 e^{j2\phi} + (j\delta - \alpha_2)^2}, \quad \alpha_m = -(-1)^n K_m.$$

3.3. Solution for $R_2 < r < R_3$

For the second grating region, the coupled mode equations are obtained by substituting Eq. (6c) into Eqs. (5) and neglecting the fast oscillating terms. As a result we have

$$\begin{aligned}\frac{da_n^{(+)}}{dr} &= \alpha_2 a_n^{(+)}(r) - (-1)^n K_m e^{j2\delta r} e^{j(\Omega_m - \phi)} a_n^{(-)}(r),\\ \frac{da_n^{(-)}}{dr} &= -\alpha_2 a_n^{(-)}(r) - (-1)^n K_m e^{-j2\delta r} e^{-j(\Omega_m + \phi)} a_n^{(+)}(r).\end{aligned} \tag{13}$$

Similarly to the former case, the solutions of Eqs. (13) can be written in the following matrix form:

$$\begin{bmatrix} a_n^{(+)}(r) \\ a_n^{(-)}(r) \end{bmatrix} = \begin{bmatrix} T''_{11}(r) & T''_{12}(r) \\ T''_{21}(r) & T''_{22}(r) \end{bmatrix} \begin{bmatrix} a_n^{(+)}(R_2) \\ a_n^{(-)}(R_2) \end{bmatrix}, \tag{14}$$

where the matrix elements $T''_{mn}(r)$ for this grating region are:

$$T''_{11}(r) = e^{j\delta(r-R_2)}\left\{\cosh[\gamma_2(r-R_2)] + \frac{\alpha_2 - j\delta}{\gamma_2}\sinh[\gamma_2(r-R_2)]\right\}, \tag{15a}$$

$$T''_{12}(r) = \frac{\alpha_m}{\gamma_2} e^{j(\Omega_m - \phi)} e^{j\delta(r+R_2)} \sinh[\gamma_2(r-R_2)], \tag{15b}$$

$$T''_{21}(r) = \frac{\alpha_m}{\gamma_2} e^{-j(\Omega_m + \phi)} e^{-j\delta(r+R_2)} \sinh[\gamma_2(r-R_2)], \tag{15c}$$

$$T''_{22}(r) = e^{-j\delta(r-R_2)}\left\{\cosh[\gamma_2(r-R_2)] - \frac{\alpha_2 - j\delta}{\gamma_2}\sinh[\gamma_2(r-R_2)]\right\}, \tag{15d}$$

with $\gamma_2 = \sqrt{\alpha_m^2 e^{-j2\phi} + (j\delta - \alpha_2)^2}$.

3.4. Threshold conditions

To find threshold conditions, we must relate waves in the central region to those in the grating region by applying proper boundary conditions. Note that these two regions

form two different waveguides. However, similar to the case of one-dimensional waveguide discontinuities, by matching the electrical and magnetic fields of the central region with those of the grating region at $r = R_1$, it is not difficult to show that in our case, the discontinuity can be described by

$$\begin{bmatrix} \tilde{a}_n^{(+)}(R_1) \\ \tilde{a}_n^{(-)}(R_1) \end{bmatrix} = \begin{bmatrix} \sqrt{C_0} e^{-j(\beta-\tilde{\beta})R_1} & 0 \\ 0 & \frac{1}{\sqrt{C_0}} e^{j(\beta-\tilde{\beta})R_1} \end{bmatrix} \begin{bmatrix} a_n^{(+)}(R_1) \\ a_n^{(-)}(R_1) \end{bmatrix} \tag{16}$$

where C_0 is the power coupling efficiency between the central region and the grating region given by

$$C_0 = \frac{4\tilde{\beta}\beta}{(\tilde{\beta}+\beta)^2} \frac{\left| \int \tilde{Z}(z) Z^*(z) \mathrm{d}z \right|^2}{\int |\tilde{Z}(z)|^2 \mathrm{d}z \int |Z(z)|^2 \mathrm{d}z}, \tag{17}$$

with Z and $\tilde{Z}$ being the slab mode distributions in two regions, respectively.

Then, taking into account Eq. (8) and (17) we have:

$$\begin{bmatrix} \tilde{a}_n^{(+)}(R_1) \\ \tilde{a}_n^{(-)}(R_1) \end{bmatrix} = \begin{bmatrix} \sqrt{C_0} e^{\alpha_1 R_1} e^{-j(\beta-\tilde{\beta})R_1} & 0 \\ 0 & \frac{1}{\sqrt{C_0}} e^{-\alpha_1 R_1} e^{j(\beta-\tilde{\beta})R_1} \end{bmatrix} \begin{bmatrix} a_n^{(+)}(0) \\ a_n^{(-)}(0) \end{bmatrix}. \tag{18}$$

Next, we assume that the phase shift in the grating regions, introduced at $r = R_2$, is small enough, so that it does not perturb the field continuity. Thus, the amplitudes of the cylindrical waves at $r = R_2$ can be found to be

$$\begin{bmatrix} \tilde{a}_n^{(+)}(R_2) \\ \tilde{a}_n^{(-)}(R_2) \end{bmatrix} = \begin{bmatrix} T'_{11}(R_2) & T'_{12}(R_2) \\ T'_{21}(R_2) & T'_{22}(R_2) \end{bmatrix} \begin{bmatrix} \tilde{a}_n^{(+)}(R_1) \\ \tilde{a}_n^{(-)}(R_1) \end{bmatrix}, \tag{19}$$

and at $r = R_3$

$$\begin{bmatrix} \tilde{a}_n^{(+)}(R_3) \\ \tilde{a}_n^{(-)}(R_3) \end{bmatrix} = \begin{bmatrix} T''_{11}(R_3) & T''_{12}(R_3) \\ T''_{21}(R_3) & T''_{22}(R_3) \end{bmatrix} \begin{bmatrix} \tilde{a}_n^{(+)}(R_2) \\ \tilde{a}_n^{(-)}(R_2) \end{bmatrix}. \tag{20}$$

Then from Eqs. (18)–(20) we obtain

$$\begin{bmatrix} \tilde{a}_n^{(+)}(R_3) \\ \tilde{a}_n^{(-)}(R_3) \end{bmatrix} = \begin{bmatrix} \hat{T}_{11}(R_3)\sqrt{C_0}e^{\alpha_1 R_1}e^{-j(\beta-\tilde{\beta})R_1} & \dfrac{\hat{T}_{12}(R_3)}{\sqrt{C_0}}e^{-\alpha_1 R_1}e^{j(\beta-\tilde{\beta})R_1} \\ \hat{T}_{21}(R_3)\sqrt{C_0}e^{\alpha_1 R_1}e^{-j(\beta-\tilde{\beta})R_1} & \dfrac{\hat{T}_{22}(R_3)}{\sqrt{C_0}}e^{-\alpha_1 R_1}e^{j(\beta-\tilde{\beta})R_1} \end{bmatrix} \begin{bmatrix} a_n^{(+)}(0) \\ a_n^{(-)}(0) \end{bmatrix}, \quad (21)$$

where the matrix $\hat{T}$ is defined by

$$\begin{bmatrix} \hat{T}_{11}(R_3) & \hat{T}_{12}(R_3) \\ \hat{T}_{21}(R_3) & \hat{T}_{22}(R_3) \end{bmatrix} = \begin{bmatrix} T''_{11}(R_3) & T''_{12}(R_3) \\ T''_{21}(R_3) & T''_{22}(R_3) \end{bmatrix} \begin{bmatrix} T'_{11}(R_2) & T'_{12}(R_2) \\ T'_{21}(R_2) & T'_{22}(R_2) \end{bmatrix}. \quad (22)$$

We assume that there is no reflection at the end of the laser structure $r = R_3$, then in order to create self-sustained oscillations, the ratio of the amplitude of the incoming-wave to that of the outgoing-wave must be zero at the boundary, *i.e.*,

$$\frac{\tilde{a}_n^{(-)}(R_3)}{\tilde{a}_n^{(+)}(R_3)} = 0. \quad (23)$$

This condition is identical to that of one-dimensional DFB laser [35]. Thus, from Eqs. (21) and (22) we obtain the eigenvalue equation of circular grating laser with the phase shift in the following form:

$$a_n^{(+)}(0)\hat{T}_{21}(R_3)\sqrt{C_0}e^{\alpha_1 R_1 - j(\beta-\tilde{\beta})R_1} + a_n^{(-)}(0)\frac{\hat{T}_{22}(R_3)}{\sqrt{C_0}}e^{-\alpha_1 R_1 + j(\beta-\tilde{\beta})R_1} = 0, \quad (24)$$

or in another form

$$C_0\begin{bmatrix} \dfrac{a_n^{(+)}(0)}{a_n^{(-)}(0)} \end{bmatrix}\begin{bmatrix} -\dfrac{\hat{T}_{21}(R_3)}{\hat{T}_{22}(R_3)} \end{bmatrix} e^{-j2(\beta-\tilde{\beta})R_1}e^{2\alpha_1 R_1} = 1. \quad (25)$$

Note that from Eqs. (19), (20), (22) and (23), we also have

$$\hat{T}_{21}(R_3)\tilde{a}_n^{(+)}(R_1) + \hat{T}_{22}(R_3)\tilde{a}_n^{(-)}(R_1) = 0, \quad (26)$$

or

$$\frac{\tilde{a}_n^{(-)}(R_1)}{\tilde{a}_n^{(+)}(R_1)} = -\frac{\hat{T}_{21}(R_3)}{\hat{T}_{22}(R_3)}. \quad (27)$$

Now, defining the reflection coefficient at $r = 0$

$$\rho_0 = \frac{a_n^{(+)}(0)}{a_n^{(-)}(0)} \quad (28)$$

and the effective coefficient of the grating seen from $r = R_1$, outwards as:

$$\rho_{R_1} = \frac{\tilde{a}_n^{(-)}(R_1)}{\tilde{a}_n^{(+)}(R_1)} e^{j\Omega_m} = -\frac{\hat{T}_{21}(R_3)}{\hat{T}_{22}(R_3)} e^{j\Omega_m}. \tag{29}$$

Then, the threshold conditions, Eq. (25) can be written in the following form:

$$C_0 \rho_0 \rho_{R_1} e^{-j\Omega} e^{2\alpha_1 R_1} = 1, \tag{30}$$

with Ω denoting the phase shift resulting from the waveguide discontinuity at $r = R_1$ (*i.e.*, between active and grating region) and from the grating shape

$$\Omega = \Omega_m + 2(\tilde{\beta} - \beta)R_1 = \frac{\pi}{\Lambda} m (W_1 + 2R_1) + 2(\tilde{\beta} - \beta)R_1. \tag{31}$$

Equation (31) is similar to the eigenvalue equation for conventional DBR laser with one perfect mirror [20]. In fact, because the field must be finite at $r = 0$, we have to require

$$a_n^{(+)}(0) = a_n^{(-)}(0), \tag{32}$$

i.e., $\rho_0 = 1$. It is also worth noting that the reflection coefficient ρ_{R_1} of the circular grating depends on the order of cylindrical waves. This can be evidenced by substituting $\hat{T}_{21}$ and $\hat{T}_{22}$, described by Eqs. (12), (15) and (22), into Eq. (29) to obtain the explicite grating reflection coefficient as

$$\rho_{R_1} = \frac{A + B}{C + D} e^{j\Omega_m} \tag{33}$$

where:

$$A = \frac{\alpha_m}{\gamma_2} e^{-j(\Omega_m + \phi)} e^{-j\delta(R_1 + R_2)} \sinh[\gamma_2(R_3 - R_2)]$$

$$\times \left\{ \cosh[\gamma_1(R_3 - R_2)] + \frac{\alpha_2 - j\delta}{\gamma_1} \sinh[\gamma_1(R_3 - R_2)] \right\},$$

$$B = \frac{\alpha_m}{\gamma_1} e^{-j(\Omega_m - \phi)} e^{-j\delta(2R_3 - R_2 + R_1)} \sinh[\gamma_1(R_3 - R_1)]$$

$$\times \left\{ \cosh\left([\gamma_2(R_3 - R_2)] - \frac{\alpha_2 - j\delta}{\gamma_2} \sinh[\gamma_2(R_3 - R_2)] \right) \right\},$$

$$C = \frac{\alpha_m^2}{\gamma_1 \gamma_2} \sinh[\gamma_1(R_3 - R_1)] \sinh[\gamma_2(R_3 - R_2)],$$

$$D = e^{-j\delta(2R_3 - R_1 - R_2)} \left\{ \cosh[\gamma_1(R_3 - R_1)] - \frac{\alpha_2 - j\delta}{\gamma_1} \sinh[\gamma_1(R_3 - R_1)] \right\}$$

$$\times \left\{ \cosh[\gamma_2(R_3 - R_2)] - \frac{\alpha_2 - j\delta}{\gamma_2} \right\},$$

The dependence on the order of cylindrical waves is represented by the factor $\alpha_m = (-1)^n$ appearing in Eq. (32). Note that all even (or odd) waves are degenerate, *i.e.*, they have the same threshold. The degeneracy among the even (odd) order cylindrical waves is a direct result of the large radius approximation for the Hankel functions. From physical argument, lower order waves should have a lower threshold, since the optical fields of the lower order waves show a better interaction with the active medium compared to the higher order ones. Recently, it has also been shown that gain saturation effect (characteristic for the laser operation above the threshold) remove [32] mode degeneracy between the cylindrical waves and fundamental cylindrical mode is preferable by laser structure. Moreover, in the case of the second order grating, for sufficient by strong coupling, radiative losses break the "longitudinal" mode symmetry improving mode selectivity [35].

4. Threshold gain of phase shift circular grating DFB/DBR lasers

In this section we present a systematic study of threshold gain and mode spectrum of circular grating lasers with additional phase shift introduced in the grating region. We confine our analysis to the first order grating resonator. Such a geometry of the structure is characteristics of CG-DFB/DBR lasers with integrated outcoupler. In these lasers, the first order grating resonator is surrounded by independent chirped outcoupling grating which focuses emitting light. On the other hand, the results presented here would provide a lower bound for second-order grating devices, since radiation effect leading to higher threshold is omitted. For the sake of convenience, we denote the position of the additional phase shift ϕ introduced by $D = R_2/(R_3 - R_1)$, the ratio of the active medium length to the grating length by $S = R_1/(R_3 - R_1)$ and the length of the grating by $L = R_3 - R_1$.

4.1. Mode spectrum and threshold gain for CG-BFB lasers with phase shift

In the case of DFB lasers, as the active medium extends under the grating region, we essentially have $\alpha_1 = \alpha_2 = \alpha$, $\tilde{\beta} = \beta$, and $C_0 = 1$.

In Figures 2–5 the normalized threshold gain αR_3 is plotted against the normalized frequency deviation δR_3 for $\Omega = 0$, and phase shift $\phi = \pi$ introduced and various position $D = 1/4$, $1/3$, $2/3$ and $3/4$, respectively. The asterisk and the circles represent the even and odd cylindrical modes, respectively. The calculation is done for $K_m L = 1$. It is seen that threshold gain as well as mode selectivity (*i.e.*, the difference

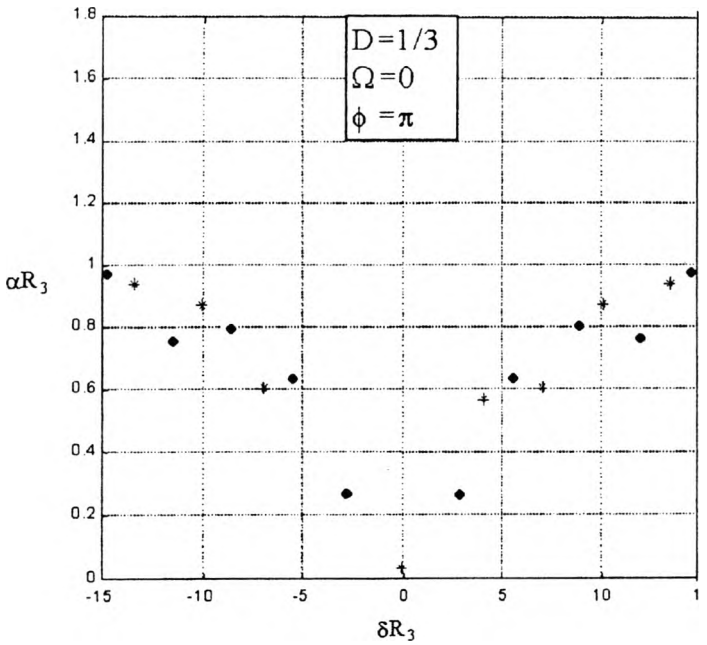

Fig. 3. Normalized small threshold αR_3 gain versus normalized frequency parameter δR_3 for CG-DFB laser with $K_m R_2 = 1.0$, $D = 1/3$ and (Ω, ϕ) equal $(0, \pi)$.

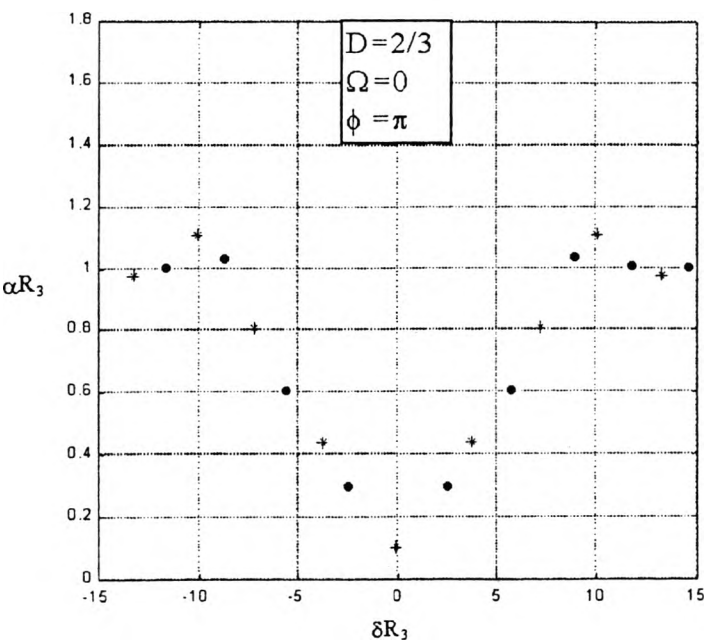

Fig. 4. Mode spectrum of CG-DFB laser with $K_m R_2 = 1.0$, $D = 2/3$ and (Ω, ϕ) equal $(0, \pi)$.

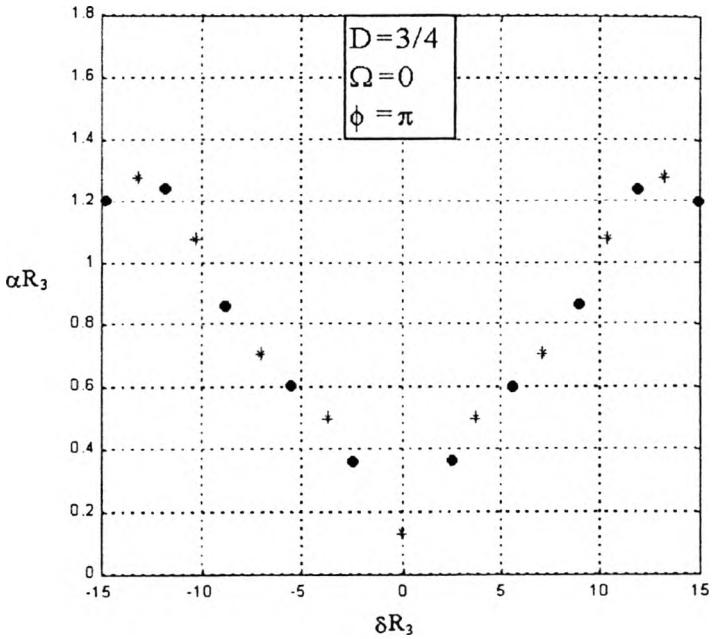

Fig. 5. Normalized small threshold αR_3 gain as a function of normalized frequency parameter δR_3 for CG-DFB laser with $K_m R_2$ = 1.0, D = 3/4 and (Ω, ϕ) equal $(0, \pi)$.

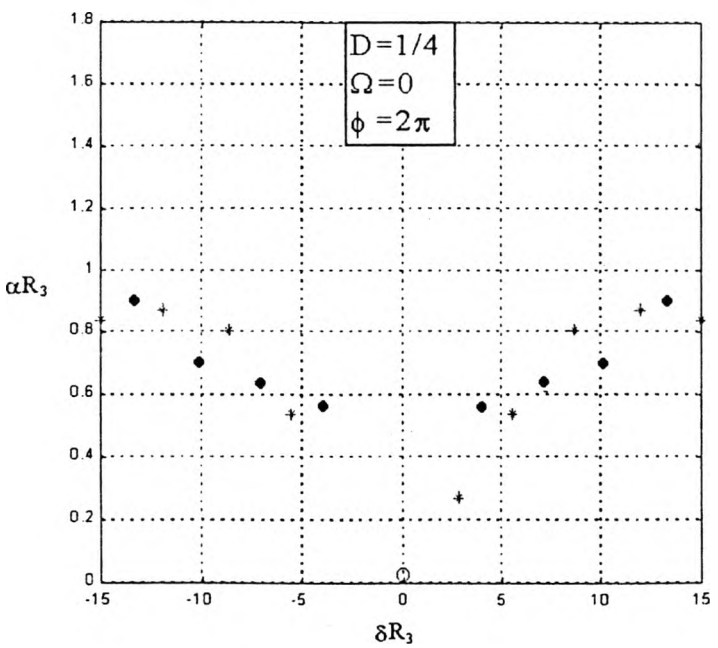

Fig. 6. Dependence of normalized threshold gain αR_3 on normalized frequency parameter δR_3 for CG-DFB laser with $K_m R_2$ = 1.0, D = 1/4 and (Ω, ϕ) equal $(0, 2\pi)$.

between the threshold gain for the fundamental and next order DFB mode) strongly depend on the position and value of the additional phase shift. Moreover, the selectivity of the laser structure can be remarkably improved in comparison to the uniform grating cavity. However, the proper choice of ϕ strongly depends of the position of grating with respect to the central point of the structure, measured by the phase Ω. Particularly, for the parameters presented in Figs. 2–5, the lowest threshold and the best mode selectivity are obtained when the phase shift is introduced at $D = 1/4$ and $D = 3/4$, *i.e.* a quarter grating length from the beginning and from the end of the grating, respectively. Moreover the parity of the lowest threshold modes can be fixed by the proper choice of the phase shifts Ω and ϕ. For example, for $\Omega = 0$ odd cylindrical modes are preferable by the laser when the additional phase shift introduced is $\phi = \pi$. The lasing frequencies of the even waves and odd waves are interchanged, when $\phi = 2\pi$, (Fig.6).

4.2. Mode spectrum and threshold gain of CG-DBR lasers with phase shift

For CG-DBR lasers, the gain region is limited within a circle of radius R_1 and the grating is a passive region with a length of $L = R_3 - R_1$. Since the grating region is independent of the active medium, we have $\alpha = \alpha_1$. In our numerical calculations, we ignore the losses in the grating region, *i.e.*, with $\alpha_2 = 0$. We also assume that $C_0 = 1$. It is worth noting here that the imperfect coupling between the gain region

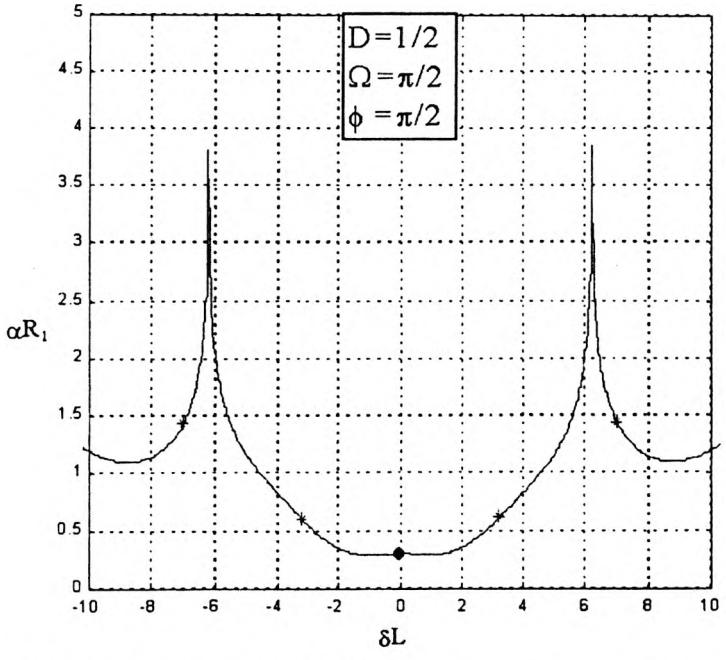

Fig. 7. Mode spectrum of CG-DBR laser with $K_m R_2 = 1.0$, $D = 1/2$ and (Ω, ϕ) equal $(\pi/2, \pi/2)$.

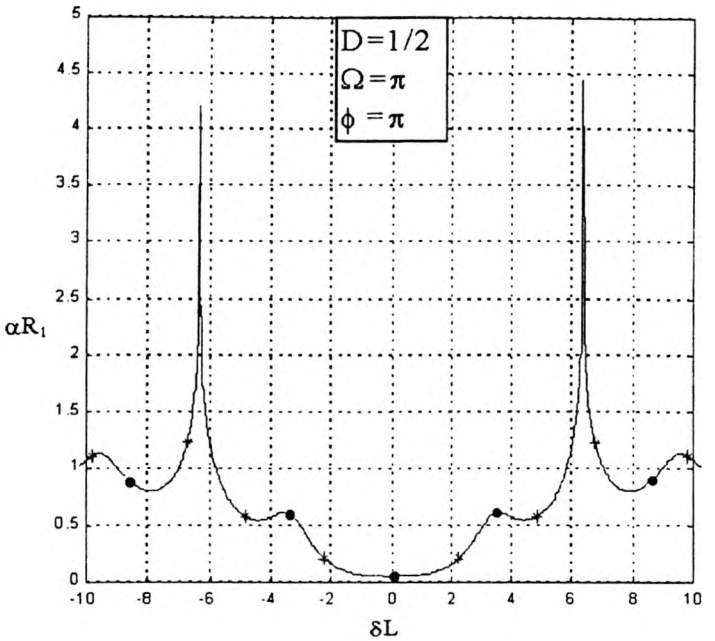

Fig. 8. Normalized small threshold αR_3 gain versus normalized frequency parameter δR_3 for CG-DFB laser with $K_m R_2 = 1.0$, $D = 1/2$ and (Ω, ϕ) equal (π, π).

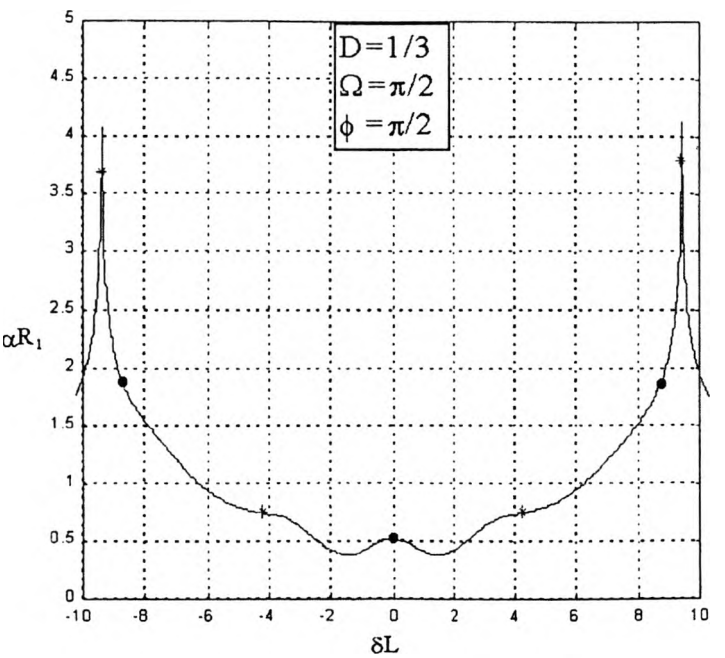

Fig. 9. Dependence of normalized threshold gain αR_3 on normalized frequency parameter δR_3 for CG-DBR laser with $K_m R_2 = 1.0$, $D = 1/3$ and (Ω, ϕ) equal $(\pi/2, \pi/2)$.

and the grating region ($C_0 < 1$) leads inevitably to additional losses, thus increasing threshold gain.

As in the case of CG-DFB laser, the mode spectrum of CG-DBR structure strongly depends on the value and the position of additional phase shift ϕ introduced in the grating region, as well as, on the phase shift Ω describing the position of the Bragg reflector with respect to the centre of the laser structure.

Figures 7 and 8 show threshold mode spectrum (*i.e.*, the normalised threshold gain α vs. normalised frequency deviation δL) for varying values of the phase shifts (Ω, ϕ), *i.e.*, (π, π) and $(\pi/2, \pi/2)$, respectively. The additional phase shift is introduced in the middle of the Bragg reflector. As we can notice, by proper choice of (Ω, ϕ) it is possible to reduce threshold gain (Fig. 8). However, in this case (*i.e.*, for $D = 1/2$), the mode selectivity of the Bragg reflector is rather weak. Thus, for such structure parameters, we can expect multimode operation above the threshold.

The influence of the position of the additional phase shift ϕ on the threshold spectrum of CG-DBR laser structure is illustrated in Figs. 9–11, where similar laser characteristics as in the previous case are presented. As with CG-DFB lasers, the mode spectrum of CG-DBR lasers is very sensitive to the position of the phase shift ϕ introduced. As we can notice, by properly choosing the position of the perturbation of the grating period, we can remarkably improve the mode selection of the Bragg reflector obtaining better condition for single mode operation. In particular, for the phase shifts equal $\Omega = \pi/2$ and $\phi = \pi/2$, respectively, the threshold gain is reduced when the grating period perturbation is introduced at $D = 2/3$ or $D = 3/4$,

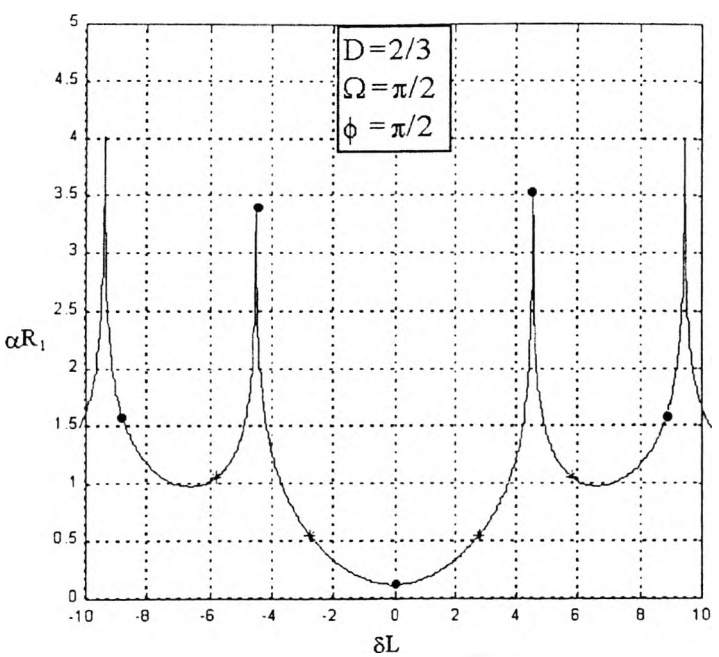

Fig. 10. Mode spectrum of CG-DBR laser with $K_m R_2 = 1.0$, $D = 2/3$ and (Ω, ϕ) equal $(\pi/2, \pi/2)$.

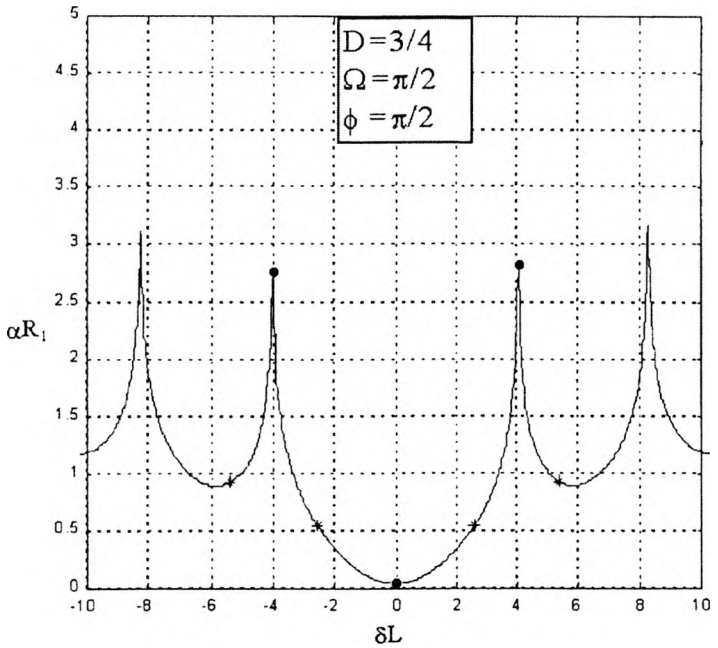

Fig. 11. Normalized small threshold αR_3 gain versus normalized frequency parameter δR_3 for CG-DFB laser with $K_m R_2$ = 1.0, D = 3/4 and (Ω, ϕ) equal $(\pi/2, \pi/2)$.

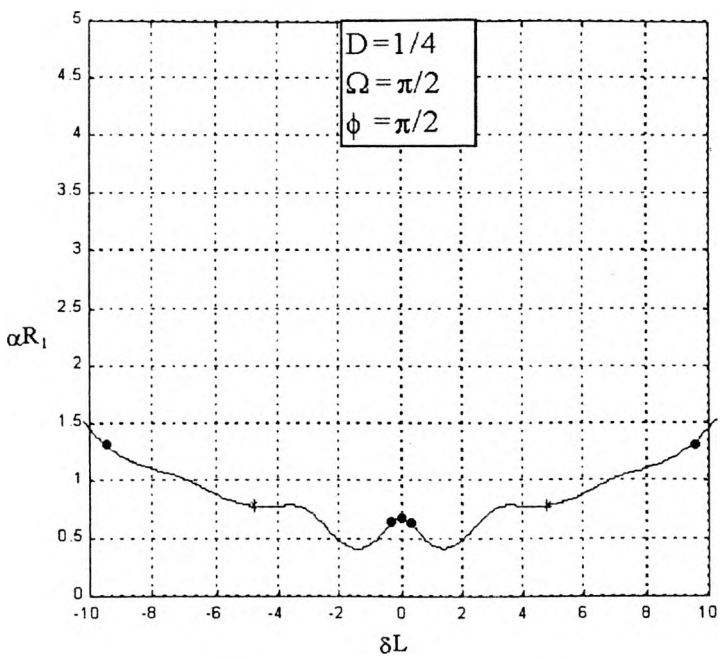

Fig. 12. Dependence of normalized threshold gain αR_3 on normalized frequency parameter δR_3 for CG-DBR laser with $K_m R_2$ = 1.0, D = 1/4 and (Ω, ϕ) equal $(\pi/2, \pi/2)$.

(see Figs. 10 and 11). It is worth noting that in this case the relatively high mode selectivity is also preserved. Thus, for this laser structure we can expect laser operation in fundamental laser mode above the threshold.

However, the improper choice of the position of the perturbation of the grating period destroys selectivity of the Bragg reflector, and oscillations on fundamental laser mode require higher gain. Such a situation is presented in Fig. 12, where the threshold mode is plotted for similar values of the phase shifts as in the previous case (*i.e.*, $\Omega = \pi/2$ and $\phi = \pi/2$), but for the different position of the perturbation introduced, $D = 1/4$. As we can notice, in this case, the mode degeneracy appears at the Bragg frequency (*i.e.*, δL), and mode selectivity of the laser structure is lost. Moreover, the threshold gain for the fundamental laser modes is increased.

5. Conclusions

In this paper we, have presented a detailed analysis for TE-laser modes in CG-DFB and CG-DBR lasers with additional phase shift introduced. Our numerical results show that by the proper choice of the inner radius of the Bragg reflector (*i.e.*, Ω), the additional phase shift ϕ introduced and its position in the grating region we can reduce the threshold gain for the fundamental laser mode. Moreover, the selectivity properties of the laser structure can also be remarkably improved in comparison with the CG-DFB/DBR having uniform Bragg reflector region, which facilitates single frequency operation.

References

[1] TIEN P. K., Opt. Lett. **1** (1977), 64.
[2] ZHENG X., Electron. Lett. **25** (1989), 1311.
[3] SHINO T., SETSUNE K., YAMAZAKI S., WASA K. Appl. Opt. **26** (1987), 587.
[4] HORI Y., SOGAWA F, ASAKURA H., *et al.*, Appl. Opt. **29** (1990), 2522.
[5] SHIMPE R. M., US patent no. 4 743 083 (1990), May 10.
[6] IP A., JACKSON D. R., IEEE Trans. Antennas and Propagations **4** (1990), 488.
[7] ALEXOPOULOS N. G., KERNER S. R., J. Opt. Soc. Am. **67** (1977), 1634.
[8] ZHENNG X., LACROIX S., J. Lightwave Techn. **10** (1990), 1509.
[9] SUDBO A. S., KAZARINOV R. F., J. Lightwave Techn. **6** (1990), 998.
[10] WU C., SILVANS M., FALLAHI M., *et al.*, Electron Lett. **27** (1991), 1819.
[11] ERDOGAN T., KING O., WICKS G. W., *et al.*, Appl. Phys. Lett. **60** (1992), 1921.
[12] ERDOGAN T., KING O., WICKS G. W., *et al.*, Appl. Phys. Lett. **60** (1992), 1773.
[13] WU C., SILVANS M., MAKINO T., *et al.*, Post deadline paper (PD3), Integrated Photonics Research Topical Meeting, New Orlean, LA, April 13–14, 1992.
[14] WU C., SILVANS M., FALLAHI M., *et al.*, Electron. Lett. **28** (1992), 1037.
[15] FALLAHI M., DION M., CHATENOUD F., *et al.*, Electron. Lett. **29** (1992), 1921.
[16] WU C., MAKINO T., DALLAHIK., *et al.*, Jpn. J. Appl. Phys. **33** (1944), L427.
[17] FALLAHI M., PEYGHAMBARIAN ., KASUNIC K., *et al.*, Electron. Lett. **32** (1996) 1583.
[18] DJALOSHINSKI L., ORENSTEIN M., IEEE J. Quantum Electron. **35** (1999), 737.
[19] KRISTJÁNSSON S., LI M., ERIKSON N., *et al.*, IEEE Photon. Technol. Lett. **9** (1997), 416.
[20] KRISTJÁNSSON S., ERIKSON N, LI M., *et al.*, IEEE J. Quantum Electron. **34** (1998), 834.
[21] KRISTJÁNSSON S., ERIKSON N, SHEARD S. J., LARSSON A., IEEE Photon. Techn. Lett. **11** (1999), 497.

[22] TODA M., IEEE J. Quantum Electron. **26** (1990), 437.
[23] ERDOGAN T., HALL D. G., J. Apll. Phys. **68** (1990), 1435.
[24] ERDOGAN T., KING O., WICKS G. W., HALL D. G., IEEE J. Quantum Electron. **28** (1992), 612.
[25] WU C., MAKINO T., GLINSKI J., *et al.*, J. Lightwave Technol. **28** (1992), 1037.
[26] WU C., MAKINO T., GLINSKI J., *et al.*, J. Lightwave Technol. **10** (1992), 1575.
[27] WU C., MAKINO T., NAJAFI S. I., *et al.*, Quantum Electron. **29** (1993), 2596.
[28] GONG X. M., CHAN A. K., TAYLOR H. F., IEEE J. Quantum Electron. **30** (1994), 1212.
[29] JORDAN R. H., HALL D., J. Opt. Soc. Am. **12** (1995), 84.
[30] KASUNIC K. J., KALLAWI M., J. Opt. Soc. Am. B **14** (1997), 2147.
[31] SHAMS-ZADEH-AMIRI, LI X., HUANG W.-P., J. Quantum Electron. **36** (2000), 259.
[32] KOSSEK T., SZCZEPAŃSKI P., J. Quantum Electron. **37** (2001), 742.
[33] GHAFOURI-SHIRAZ H., LO B. S. K, *Distributed Feedback Lasers – Principles and Physical Modelling*, [Ed.] Wiley, 1996.
[34] KOGELNIK H ., SHANK C. V., J. Appl. Phys. **43** (1972), 2327.
[35] GREENE P. L., HALL D. G., IEEE J. Quantum Electron. **37** (2001), 365.
[36] *Ibidem*, p. 353.

Received April 23, 2001
in reviced form May 31, 2001